Broadband radar cross-section reduction via a 1-bit coding metasurface at terahertz frequencies

MA HONG-YU[a], CHEN ZHI-HONG[a,*], LIU SHENG-YU[b,*], REN GUANG-JUN[a,*], ZHANG HAI-WEI[a], YAO JIAN-QUAN[c]

[a]*School of Electrical and Electronic Engineering, Tianjin Key Lab of Film Electronic & Communication Devices, Tianjin University of Technology, Tianjin 300384, PR China*

[b]*School of computer Science, Faculty of Engineering, The University of Sydney, Sydney 2006, NSW, Australia*

[c]*College of Precision Instrument and Opto-electronics Engineering, Institute of Laser and Opto-electronics, Key Laboratory of Optoelectric Information Science and Technology, Ministry of Education, Tianjin University, Tianjin 300072, PR China*

Broadband terahertz radar cross-section (RCS) reduction is achieved via a 1-bit coding metasurface. The proposed electromagnetic metasurface consists of two basic digital elements. The 180° phase difference between the neighboring elements can realize the reduction of RCS by a non-directional low-scattering of the broadband THz frequency. The calculated results show that the RCS reduction can be up to 15-26 dB in most of the wide frequency range of 0.7-1.6 THz. Compared to the existing research results, the metasurface for RCS reduction is non-directional and has the characteristics of broad-band and low-scattering.

(Received September 30, 2019; accepted June 16, 2020)

Keywords: Coding metasurface, Diffuse reflection, RCS, Terahertz

1. Introduction

Terahertz (THz) waves, located in the gap between microwaves and infrared optics [1], have many advantages including high resolution, non-ionizing radiation and good penetration into non-conducting materials. Compared with other frequency bands, THz can also carry and transmit more information [2-4]. Therefore, the application of THz in high performance broadband transmission equipment (such as beam scanning equipment, insulators and plasma lenses) has been put forward with higher requirements [5]. In these applications, THz radar presents more advantages than microwave radar systems in terms of aviation and military security because of its extremely wide band and high spatial resolution [6-9]. Considering these applications also need to effectively control the EM wave energy using a low reflection metasurface [10-14], the innovative research and design of low-scattering metasurfaces have been promoted. In order to reduce the RCS, some kinds of designs have been proposed to absorb broadband EM waves in the THz range [15-18]. Liu et al. proposed a broadband THz absorber by multi-layers [19], while Ye et al. proposed a polarization-insensitive and broadband THz absorber using I-shaped resonators [20]. Though the EM wave is easily consumed by the metallic surface and dielectric isolation layer and transformed into thermal radiation, the possibility of detection by an infrared detector will inevitably increase [21], with the temperature of the object increases. Hence, it is an important challenge to design a broadband, low-scattering, non-absorptive metasurface in the THz range.

Metasurface is an artificial layered material that consists of periodic or quasi-periodic two-dimensional planar arrays of sub-wavelength elements. These materials have special electromagnetic properties that cannot be normally found in natural materials that exit in nature [22-25]. It can be employed to control the polarization, amplitude, phase, propagation modes of the EM wave. In 2008, Liu et al. designed a kind of metasurface that covers the metal plate to appear diffuse reflection of reflected wave, which is successfully suppressed backward scattering [26].

In 2014, Professor Cui Tiejun proposed a phase-encoded metamaterial based on phase mutation control, which uses discrete digital coding to characterize each sub-wavelength unit structure, it can be combined with optimization algorithms, and have more freedom to regulate the EM waves [27]. These particular metasurfaces may greatly simplify the design and enhance the all-around flexibility to regulate the EM waves. Therefore, metasurfaces are meaningful for designing various devices in different frequencies band (i.e., from microwaves to the visible region), especially within the THz gap [28].

In this paper, we designed a non-directional, broadband low-scattering metasurface by coding the “0” and “1” digital elements at THz frequencies. The wideband low-scattering is attributed to the reflection phase differences between the two basic digital elements,

which makes it different from the traditional metamaterial devices. Though optimizing the structure of the basic element, the energy reflected from the metasurface can be scattered into various directions, resulting in the low intensity and uniform distribution of the reflected wave. The simulation results show that the RCS reduction of the metasurface relative to the same size metal plate is more than 10 dB from 0.7 THz to 1.6 THz. Therefore, it can achieve a wider bandwidth and a larger RCS reduction, and it presents considerable prospects in THz radar, broadband communication, military security and other applications.

2. Theory

RCS is a physical quantity used to represent the echo intensity of a target under the irradiation of radar waves [29], it has important guiding significance for radar systems design, target recognition, tracking point selection and stealth technology [30]. The RCS is defined as:

$$\sigma = \lim_{R\to} 4\pi R^2 \left|\frac{E_s}{E_i}\right|^2 \quad (1)$$

where E_i represents the intensity of the electric field projected on the target, E_s represents the intensity of the radar target scattering wave, R represents the distance from the radar to the target scatter. The smaller the target's RCS is, the less echo energy the radar receives, thus achieving the goal of stealth [31]. The basic principle is based on the theory of reflection array antenna of the metasurface proposed in this paper [32]. Through the design of coding arrangement, the incident EM wave is diffusely reflected, that is, it is not absorbed or lost, but scattered in all directions, forming numerous scattered waves. Assuming that there is a coding metasurface composed of N × N array elements as shown in Fig. 1, each of the array consists of two basic elements, "0" and "1". In the case of normal incidence of electromagnetic waves, the far-field scattering of the surface can be expressed as:

$$f(\theta,\varphi)=f_e(\theta,\varphi)\sum_{m=1}^{N}\sum_{n=1}^{N}\exp\left\{-i\left\{\varphi(m,n)+kd\sin\left[\left(m-\frac{1}{2}\right)\cos\varphi+\left(n-\frac{1}{2}\right)\sin\varphi\right]\right\}\right\} \quad (2)$$

where θ and φ are the angle of incidence and azimuth respectively; $k = 2\pi/\lambda$; d is the distance between each unit; $f_e(\theta, \varphi)$ is the radiation intensity of each element, the directional graph function can be expressed as:

$$\mathrm{Dir}(\theta-\varphi)=\frac{4\pi\left|f(\theta,\varphi)^2\right|}{\int_0^{2\pi}\int_0^{\pi/2}\left|f(\theta,\varphi)^2\right|\sin\theta d\theta d\varphi} \quad (3)$$

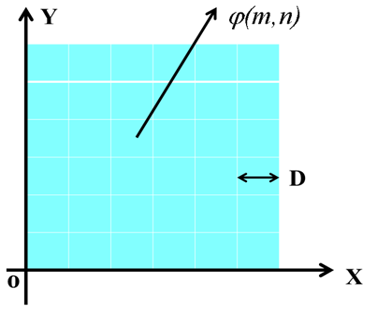

Fig. 1. The diagram of the electromagnetic metasurface, which contains N × N lattices with size D, in which each lattice is occupied by a "0" and "1" elements (color online)

Due to a phase gradient of 180° can be formed by the element 0 and 1, the scattering characteristics can cancel each other out, which makes the radiation characteristics of the $f_e(\theta, \varphi)$ be zero basically. From the above two formulas, it can be found that the far-field scattering properties of the metasurface will change with the arrangements of the coding array.

The proposed 1-bit coding metasurface is shown in Fig. 2(a). As it is illustrated in the figure, the digital elements are randomly arranged to diverse 0-1 sequence to achieve the desired diffuse scattering. The size of the total metasurface unit structure is 1.1 mm × 1.1 mm, which includes 10 × 10 coding particles. The basic digital elements of the 1-bit coding metasurface are "0" and "1", and the distance between two adjacent elements is P=110 μm as shown in Fig. 2(b). The "0" element was realized using no metallic structure, while "1" was realized using a three-layer structure which was composed of the metal ring surface, dielectric polyimide (PI) and the metal substrate from top to bottom. Among them, polyimide is a lightweight, high temperature resistant structural material and an excellent insulating dielectric material, and according to the needs of the experiment, it can be formed into a thin film or a thick film. Both the substrate and surface metals were gold with a thickness of 0.2 μm, and the PI has a thickness of h = 40 μm with a dielectric constant 3.1 and a loss tangent 0.05. For the "1" element, $w = 5.5\ \mu m$, r1=37 μm and r2=31.5 μm as shown in Fig. 2(c).

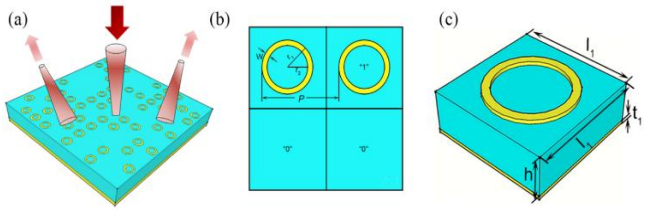

Fig. 2. (a) Schematic of a 1-bit coding metasurface. (b) Schematic of adjacent metal square ring. (c) Dimension drawing of unit structure (color online)

In order to understand the properties of the basic digital elements more intuitively, numerical simulation results were performed by CST Microwave Studio, as shown in Fig. 3(a). Simulation software is used to calculate the reflection phase of the structure, the reflection phase difference of the "0" and "1" structures is close to 180° between the 1.0 THz ~1.6 THz, the range of variation is 180° ± 30°. The proposed 1-bit coding metasurface structure is composed of the aperiodic coding sequence "0001101101 ...". It is assumed that the coded metasurface is a one-dimensional code sequence along the x-axis in order to calculate the scattering field of different sequence coded metasurfaces and analyze the scattered waves more clearly, as shown in Fig. 3(b).

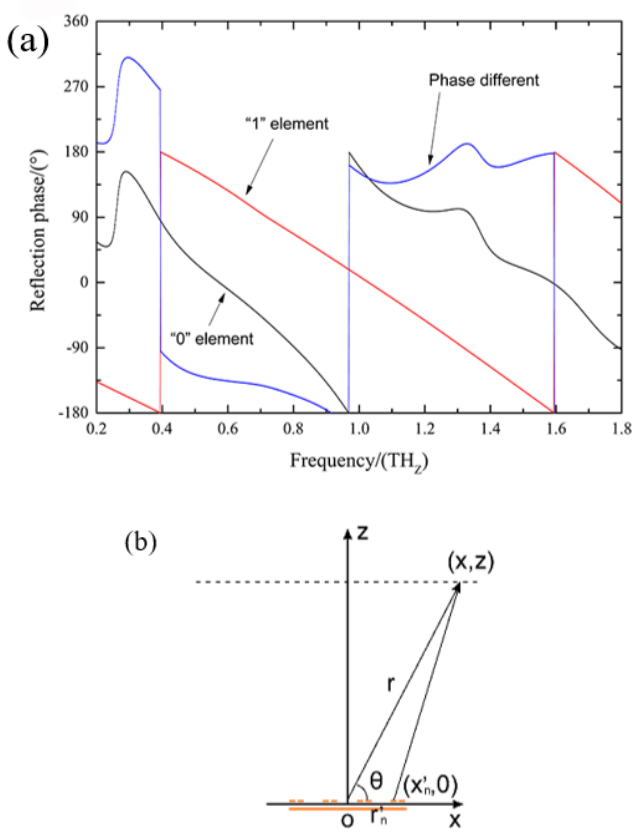

Fig. 3. (a)The reflected phase difference of the "0" and "1" element in a range THz frequency. (b) Schematic of the 1D coding metasurface (color online)

The scattering behaviors can also be interpreted by simple theory, by Treating "0" and "1" elements as the dipole radiation source, the far-field radiation in the top half space is given by, where A is the complex scattering amplitude vector. The overall electric field at a far field position r can be expressed as the sum of the sources (neglecting the factor the $e^{-i\omega t}$):

$$E=\sum_n A_n e^{ik(r-r_n')}=\sum_n A_n e^{i\frac{2\pi\sin\theta(x-x_n')+2\pi\cos\theta\cdot z}{\lambda}} \quad (4)$$

where n indicates the nth dipole radiation source and x_n' is the position coordinate of the nth dipole radiation source. This may be caused by the assumption of spherical radiation of the sources. The formula (3) implies that anomalous behaviors come from the superposition of radiation from each "0" and "1" digital element. The broadband of the low-scattering coefficient of the coding metasurface was realized by optimizing the sequences of the basic elements, and the proposed metasurface was constructed with a single metallic structure layer. Thus, the proposed metasurface is easier to fabricate than other multi-layer metasurfaces.

3. Results and discussion

Full-wave simulation of coded 1-bit electromagnetic metasurface is carried out using electromagnetic field CST Microwave Studio. In the case of normal incidence, the relationship between frequency and reflection of the metasurface THz wave designed in this paper is shown in Fig. 4. The reflection is lower than -10 dB in the bandwidth from 1.0 THz to 1.6 THz, this result is consistent with the bandwidth range of the fundamental phase difference between the two basic digital elements of "0" and "1", and the reflection even reached -25 dB at f=1.3 THz. Therefore, the designed 1-bit coded metasurface implements the low reflection effect of the broadband image.

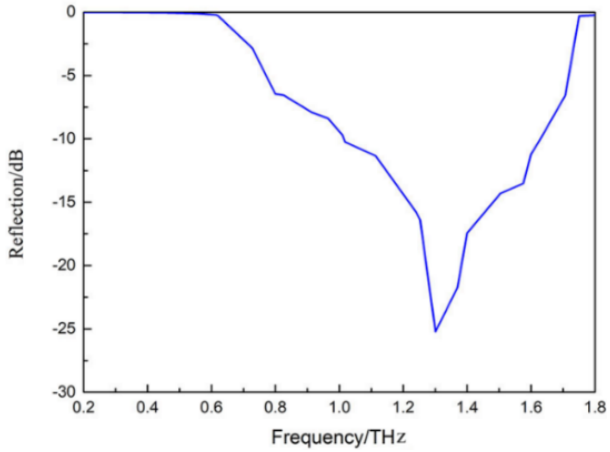

Fig. 4. The simulation curve for 1-bit coding metasurface THz wave frequency and reflection under the normal incidence

In order to understand the scattering properties of the electromagnetic coding metasurface, formula (4) is used to calculate the scattering characteristics of the coded metasurface by different sequences of "000111000111..." and "001001001..." at f = 1.3 THz, as shown in Fig. 5(a), for "000111000111..." coded metasurface, the number of scattered waves is two, while for "001001001..." coded metasurface, the number is three. In addition, the angle at which the two scattered waves is determined by θ = ± arcsin (λ/4P) for the "000111000111...", where λ is wavelength, the angle of the three scattered waves is determined by θ = 0 and θ = ± arc sin(λ/3P), and the far-field scattering characteristics of "000111000111..."

and “001001001...” period coded metasurface at f = 1.3 THz are shown in Fig. 6. It can be seen from it that the THz coded metasurface scattering beams are 2 and 3 beams respectively. In this paper, the proposed 1-bit coded metasurface structure is composed of the quasi-periodic coding sequence "0001101101 ...". Formula (4) is used to calculate the scattering characteristics of the coded metasurface. As shown in Fig. 7. It is known that the coded metasurface structure has countless scattering beams, and the scattering is non-directional, so the reduction of RCS can be achieved. The far-field scattering characteristics of aperiodic coding metasurface at different frequencies are shown in Fig. 8. It can be seen from it that the bandwidth range of the reflection below -10 dB is 1.0 THz ~1.6 THz, the backward RCS distributed on the metasurface in spray shape, and the beam of the scattered wave is innumerable. At the same time, the energy of the electromagnetic wave is dispersed in all directions, and the energy of each wave is very low. The simulation results are basically consistent with the theoretical calculation, which further proves the accuracy of theoretical calculation. Therefore, it can achieve the goal of reducing RCS.

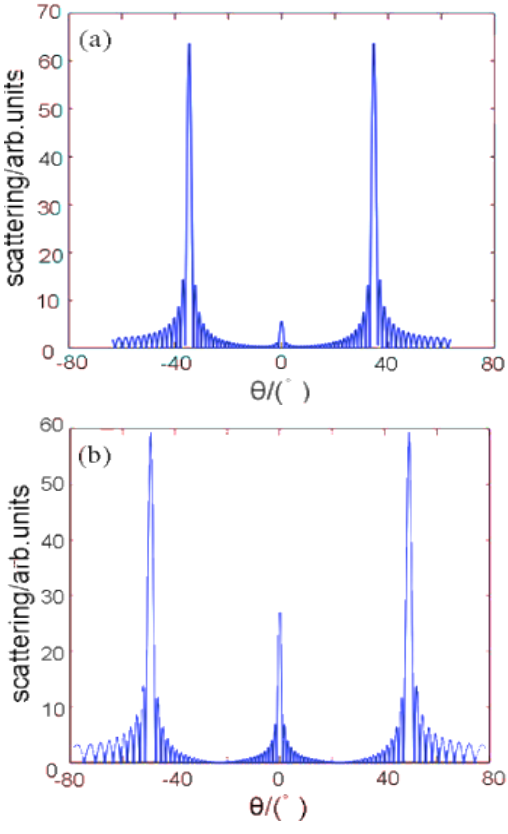

Fig. 5. (a) 1d “000111000111...” coding sequence metasurface scattering characteristics. (b) 1d “001001001...” encoding sequence metasurface scattering characteristics

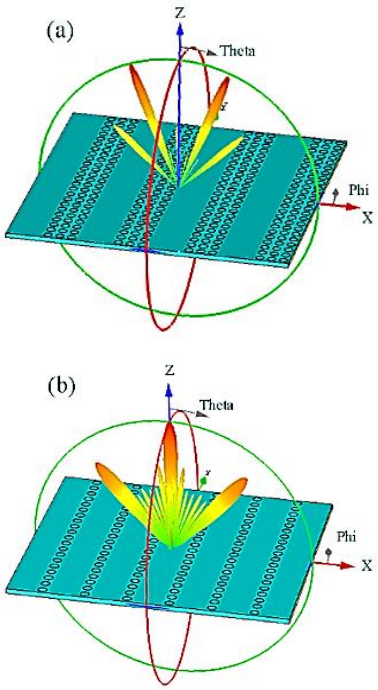

Fig. 6. Simulation far-field patterns of the scattering results of: (a) “000111000111…” (b) “001001001…” at 1.3 THz for coding metasurface (color online)

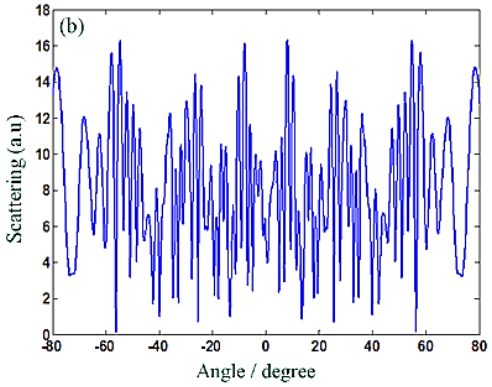

Fig. 7. 1d “0001101101...” coding sequence metasurface scattering characteristics (color online)

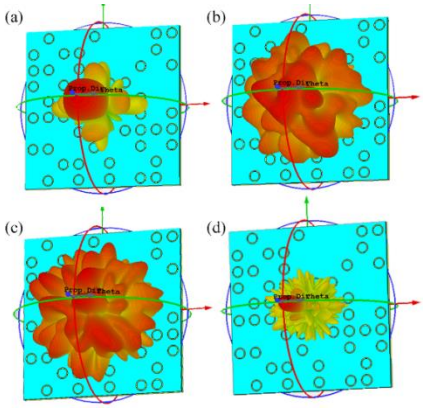

Fig. 8. Simulation far-field patterns of the scattering results of coding metasurface at (a) 0.6 THz; (b) 1.0 THz; (c) 1.3 THz; (d) 1.6 THz (color online)

The backward RCS is conical at f = 0.6 THz and f = 1.6 THz in Fig. 8, and the scattered waves are not dispersed to all directions, the effect of diffuse reflection is not achieved. This is because the reflection phase difference between the two structures of "0" and "1" at these two frequencies deviated by 180°, so the scattering characteristics of the two structures are mutually offset and weaken.

In order to more clearly observe the far-field transparency effect of the coded metasurface, the transparency properties of the metasurface and metal plate were compared quantitatively. The transparency patterns in the x z-plane obtained along a line passing through the middle of the surfaces (i.e., y = 0 [the x o z-plane]) were obtained by simulation at 0.6 THz, 1.0 THz, 1.3 THz, and 1.6 THz, and the patterns for the metasurface and the metal plate as shown in Fig. 9. According to the law of energy conservation, The RCS reduction of the metasurface must have a repressed the main lobe and enforced side lobes to maintain the overall scattering energy. Indeed, it can be observed in Fig. 9(e-h) that a strong main lobe appears in the backward direction for the metal plate at the full working band. It can be observed in Fig. 9(c, d, g, h) that the metasurface is suppressed the main lobe energy and uniformly scattered energy to the side lobes at 1.3 THz and 1.6 THz relative to the metal plate. Therefore, the simulation results further indicate that the coded metasurface achieves the effect of reducing RCS.

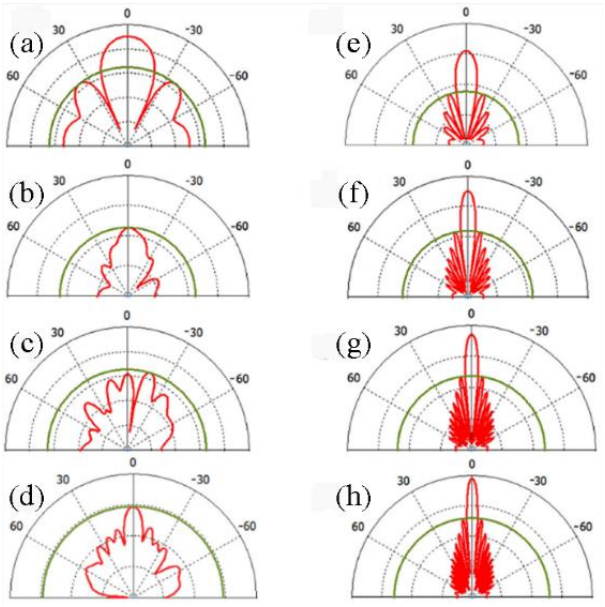

Fig. 9. Scattering patterns of the coding metasurface in the XOZ-plane at (a) 0.6 THz, (b) 1 THz, (c) 1.3 THz, (d) 1.6 THz. Scattering patterns of the metal plate in the XOZ-plane at (e) 0.6 THz, (f) 1 THz, (g) 1.3 THz, (h) 1.6THz (color online)

Fig. 10 shows the RCS reduction of the coded metasurface relative to the same size metal plate when the electromagnetic wave is incident vertically. It can be found that the RCS reduction of the coded metasurface relative to the metal plate exceeds 10 dB at the 0.7 THz ~1.6 THz, so it has broadband features, and these features are basically the same as the bandwidth of the reflection phase difference between the "0" and "1" units. The RCS reduction can be up to 26 dB when f = 1.3 THz, with an extremely low reflectivity.

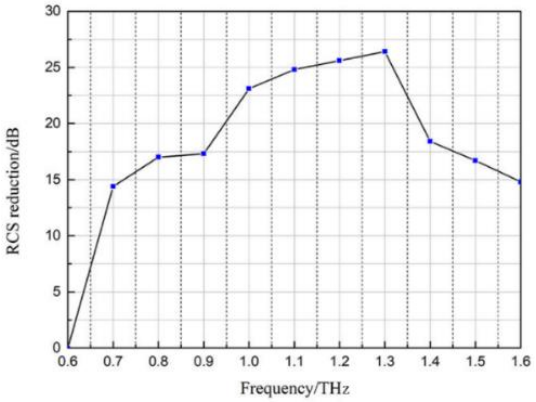

Fig. 10. The RCS reduction of the coded metasurface relative to the same size metal plate when the electromagnatic wave is incident vertically

4. Conclusion

In our paper, we proposed a non-directional low-scattering 1-bit coding metasurface that can reduce the RCS in THz band. The numerical simulated results indicate that the scattering wave of the coded metasurface possesses the diffuse reflection effect with a reflection lower than -10 dB in the frequency range of 0.7-1.6 THz. Compared with metal plates of the same size, the RCS reduction of the coded metasurface reaches 15-26 dB at 0.7 ~ 1.6 THz. The operating bandwidth of the coded metasurface is practically the same as the bandwidth of the reflection phase difference between the "0" and "1" elements. Therefore, the proposed coded-metasurface is an efficient broadband backward RCS reduction structure, and it is expected to present considerable application prospects in THz radar stealth, military security and biomedical imaging.

Acknowledgements

National Natural Science Foundation of China (grant number 61505144), the Tianjin Research Program of Application Foundation and Advanced Technology (grant number 14JCQNJC00900), the National key Research and Development Program of China (Grant N0. 2017YFA0700202), the Scientific Research Project of Tianjin Municipal Education Commission (Grant No.

2018KJ136) and the Natural Science Foundation of Tianjin (Grant No. 18JCQNJC71200).

References

[1] B. Ferguson, X. C. Zhang, Physics **1**(1), 26 (2002).
[2] P. H. Siegel, IEEE Transactions on Microwave Theory & Techniques **50**(3), 910 (2002).
[3] M. I. Lvovska, N. C. Seeman, R. Sha et al., IEEE Transactions on Nanotechnology **9**(5), 610 (2010).
[4] L. Xie, Y. Yao, Y. Ying, Applied Spectroscopy Reviews **49**(6), 448 (2014).
[5] I. F. Akyildiz, J. M. Jornet, C. Han, Physical Communication **12**, 16 (2014).
[6] B. Zhang, Y. M. Pi, J. Li, Sensors Journal, IEEE **15**(1), 290 (2015).
[7] H. S. Lui, T. Taimre, K. Bertling, Optics Letters **39**, 2629 (2014).
[8] K. B. Cooper, R. J. Dengler, N. Llombart, Journal of Infrared Millimeter & Terahertz Waves **30**(12), 1297 (2009).
[9] K. B. Cooper, R. J. Dengler, N. Llombart, IEEE Transactions on Terahertz Science & Technology **1**(1), 169 (2011).
[10] P. U. Jepsen, D. G. Cooke, M. Koch, Laser & Photonics Reviews **6**(3), 418 (2012).
[11] T. Kleine-Ostmann, T. Nagatsuma, Journal of Infrared Millimeter & Terahertz Waves **32**(2), 143 (2011).
[12] M. Y. Liang, C. L. Zhang, R. Zhao, Journal of Infrared Millimeter & Terahertz Waves **35**(9), 780 (2014).
[13] R. Singh, W. Cao, I. Al-Naib, Applied Physics Letters **105**(17), 1 (2014).
[14] L. Xie, W. Gao, J. Shu, Scientific Reports **5**, 8671 (2015).
[15] H. Hua, Y. S. Jiang, Y. He, Progress in Electromagnetics Research B **59**(A12), 193 (2014).
[16] S. L. He, T. Chen, IEEE Transactions on Terahertz Science & Technology **3**(6), 757 (2013).
[17] J. Zhu, Z. Ma, W. Sun, Applied Physics Letters **105**, 021102 (2014).
[18] Y. Shen, Z. Pei, Y. Pang, Journal of Applied Physics **117**(22), 224503.1 (2015).
[19] S. Liu, H. B. Chen, T. J. Cui, Applied Physics Letters **106**(15), 151601 (2015).
[20] Y. Q. Ye, Y. Jin, S. L. He, JOSA B **27**, 498 (2010).
[21] B. X. Wang, L. L. Wang, G. Z. Wang, Applied Physics A **115**, 1187 (2014).
[22] C. L. Holloway, E. F. Kuester, J. A. Gordon, IEEE Transactions on Antennas & Propagation **60**(11), 5173 (2012).
[23] Y. M. Liu, X. Zhang, Applied Physics Letters **103**(14), 141101-5 (2013).
[24] L. Liu, X. Zhang, M. Kenney, Advanced Materials **26**(29), 5031 (2014).
[25] K. Wang, J. Zhao, Q. Cheng, D. S. Dong, T. J. Cui, Scientific Reports **4**, 5935 (2014).
[26] S. Liu, H. B. Chen, T. J. Cui, Applied Physics Letters **106**(15), 151601 (2015).
[27] T. J. Cui, M. Q. Qi, X. Wan, Light Science & Applications **3**(10), e218 (2014).
[28] L. Huang, X. Chen, B. Bai, Light: Science & Applications **2**(3), e70 (2013).
[29] E. F. Knott, J. F. Schaeffer, M. T. Tulley, "Radar Cross Section, 2nd Edition", Scitech Publishing, 644 (2004).
[30] V. S. Chernyak, "Fundamentals of Multisite Radar Systems: Multistatic Radars and Multistatic Radar Systems", CRC Press, 492 (1998).
[31] M. A. Richards, Fundamentals of Radar Signal Processing, 2e[M]. (2005).
[32] T. J. Cui, M. Q. Qi, X. Wan et al., Light Science & Applications **3**(10), e218 (2014).

*Corresponding author: zhchen@email.tjut.edu.cn
shengyuliu558@163.com
rgj1@163.com